Propagation of near-inertial waves beneath atmospheric storm tracks on the non-traditional β-plane

Marine Tort and Kraig B. Winters

Scripps Institution of Oceanography,
University of California San Diego
mtort@ucsd.edu

Abstract

We present results of 2d, in the meridional-depth plane, and 3d numerical simulations of near-inertial waves (NIWs) propagating in a stratified, turbulent mid-latitude ocean on the non-traditional (NT) β-plane. Here NT refers to the retention of the horizontal component of the Coriolis force. Continuous surface wind forcing, containing both high- and low-frequency components produces propagating NIWs and a baroclinic unstable zonal jet, sustaining an active field of mesoscale eddies in 3d. In 2d, most of the NIWs propagate equatorward, with poleward propagating waves being reflected back toward the equator at a nearby turning latitude. With NT effects included, waveguides exist that permit weak sub-inertial wave poleward propagation. In 3d, a poleward energy flux, carried by super-inertial internal waves, is found to be as strong as the equatorward flux. These results suggest that, while the inclusion of NT effects permits sub-inertial wave propagation, fluctuating zonal winds over an eddying ocean do not excite these motions very strongly.

1 Introduction

NIWs are rapidly oscillating waves generated by wind bursts at the ocean surface that significantly contribute to the interior ocean mixing required to maintain the global meridional overturning circulation (Garrett and Munk, 1972). These waves transfer energy from large to small scales, where the energy is converted into heat through dissipation and potential energy through diapycnal mixing. It is unclear however what fraction of the energy input at the sea surface is actually available for ocean mixing and how the cascade to smaller scales and mixing occurs. NIWs may spread both horizontally and vertically into the interior, but only when their horizontal scale is much smaller than the wind scales. Two mechanisms significantly reduce the initially large scales of these wind-driven motions: (1) the β-effect (e.g. D'Asaro 1989) which can reduce infinite scales to $R_d = O(100)$ km in about $t = 2\pi/(\beta R_d) = 40$ days and (2) the relative vorticity gradient $\nabla\zeta$ (Kunze, 1985) which may be a much more efficient mechanism to generate small scales than (1) if $\nabla\zeta \gg \beta$. Those two effects also alter the propagation of the NIWs.

(1) Within the traditional approximation (TA), when the near-inertial (NI) energy has been drained from the surface to the interior, all energy radiated from the source eventually propagates towards the equator, with the initial poleward propagation being reflected at the inertial latitude due to the β-dispersion effect (e.g. Anderson and Gill 1979; Garrett 2001). While relaxing the TA, the allowed frequency range is enlarged and the NIWs can propagate sub-inertially beyond the inertial latitude. The combined effects of the NT Coriolis force and weak stratification leads to the existence of waveguides for sub-inertial waves, which get trapped and propagate poleward (Gerkema and Shrira, 2005b,a; Winters et al., 2011).

(2) Small-scale NI motions which are distorted by mesoscale eddies are "polarized" and more specifically are expelled from cyclonic eddies and trapped within anticyclonic ones (e.g. Young and BenJelloul 1997; Klein and Smith 2001). Acting as a conduit to the deep ocean, the presence of anticyclonic eddies strongly enhances the leakage of NI energy out of the surface layer through the "chimney effect" of Lee and Niiler (1998).

Wind-driven NIW propagation in an ocean basin with a baroclinically unstable zonal jet responsible for a turbulent mesoscale eddy field is studied in numerical simulations on the NT β-plane. Here, the β-effect and the mean vorticity gradient of the zonal jet have comparable effect on reducing NIW length scales i.e. $\nabla\zeta_{\text{jet}}/\beta = O(1)$. The horizontal gradient of the mesoscale eddy field may generate much smaller scales since $\nabla\zeta_{\text{eddies}}/\beta = O(100)$ and wave trapping could occur. We focus on the propagation of the waves under the influence of NT dynamics, the unstable zonal jet and associated mesoscale eddies.

2 Methods

A near-inertial propagating wave field interacts with a non-linear baroclinically unstable jet in a zonal β-plane channel centered at $\phi_0 = 45°$N. The domain size is $L_x = 400$ km in the zonal direction, $L_y = 2000$ km in the meridional direction, and its depth is $L_z = 4$ km. The 3d Boussinesq equations including both traditional $f = f_0 + \beta y = 2\Omega \sin\phi_0 + \beta y$ and NT $\tilde{f} = 2\Omega\cos\phi_0$ Coriolis parameters are solved using the 3D spectral model `flow_solve` (Winters and de la Fuente, 2012). A zonal and meridional wind body force is applied at the surface and confined in the meridional direction to the center of the domain. On one hand, the internal NIW field is excited by the stochastic part (high-frequency, HF) of zonal and meridional wind forcing. On the other hand, the mesoscale flow is generated by the steady (low-frequency, LF) component of the zonal wind. The model is periodic in the zonal direction and outward radiating waves are damped in sponge regions adjacent to the lateral boundaries via Rayleigh damping. High-order horizontal "hyperdiffusion" terms are added to the momentum and buoyancy equations to remove energy as close as possible to the grid scale and linear bottom drag is applied at the bottom to arrest the inverse cascade.

We first integrate the equations for 3 years in a 2d meridional-depth plane assuming either $\tilde{f} = 0$ or $\tilde{f} \neq 0$. An ocean at rest with a depth- and meridional-dependent density field is considered as an initial condition. After 3 years of integration, a baroclinic jet surface intensified with a maximum speed of 50 cm/s (Fig. 1a) is produced. The resulting mean potential vorticity gradient (Fig. 1b) has a zero crossing at about -1000 m. The jet is thus subject to the baroclinic instability associated with the zero crossing, which is typical of a baroclinic instability of the Phillips type. We restart the 3d runs using the final state of the 2d runs, extended and perturbed in the zonal direction. After about 90 days the most unstable mode has saturated and eddies start to be expelled from the jet.

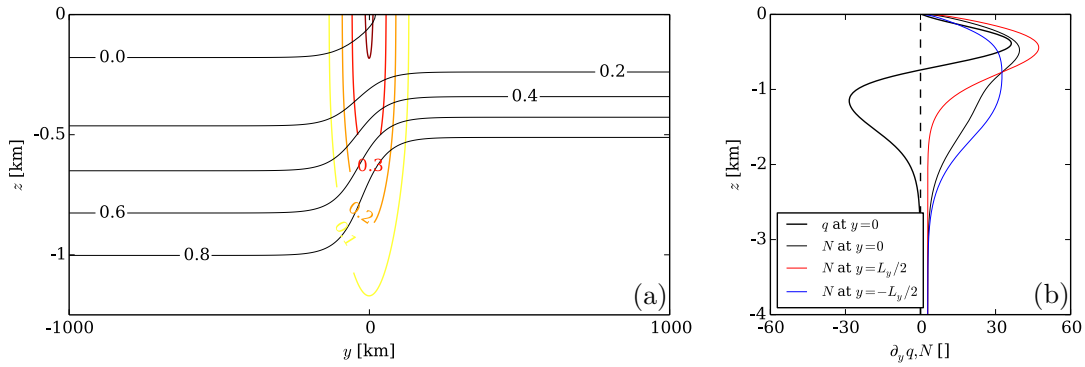

Figure 1: Baroclinically unstable background jet characteristics. (a) Time-averaged background jet profile, where the zonal velocity $\overline{u}(y,z)$ (m/s) is super-imposed by the density field $\overline{\rho}(y,z)-\rho_0$ (kg/m^3). (b) Normalized Brunt-Väisälä frequency at the central meridional location (black), at the northern most location (red) and at the southern most location (blue). The dimensionless meridional gradient of potential vorticity at the central meridional location is shown in solid thick black line.

runs	**approximation**	**number of grid points** $n_x \times n_y \times n_z$	**time stepping** dt (s)
2d-r1	TA and NT	$1 \times 321 \times 257$	240
2d-r3	TA and NT	$1 \times 1281 \times 513$	60
3d-r1	TA and NT	$64 \times 321 \times 257$	240
3d-r2	NT	$128 \times 641 \times 513$	120
3d-r3	NT	$256 \times 1281 \times 513$	60

Table 1: Parameters defining the different runs.

The statistically steady state of run 3d-r3 (NT) is obtained by running multiple nested simulations (Tab. 1). A 5-year low resolution simulation has first been run (run 3d-r1 NT) from the final state of run 2d-r1 (NT). After a spin-up of 2 years, the total kinetic energy has saturated, although its time evolution during the next 3 years is still affected by low-frequency variations with weak amplitudes. The final state of run 3d-1 (NT) is interpolated on a finer grid to restart a higher resolution simulation (run 3d-r2 NT), in which small-scale motions are rapidly produced and a steady-state is quickly attained (in 6 months). A third run (run 3d-r3) has been run for 6 months restarting from run 3d-r2 (NT). Figure 2 shows representative snapshots of the vertical component of surface vorticity normalized by f_0 (Rossby number) for the different nested runs. The mesoscale flow and NIW field have been in adjustment for 3 years after destabilization for runs 3d-r1 and for 4 years for run 3d-r3. A statistical analysis is done over 30 days after the system has reached steady state and output data are saved every 10 mins. In the following section, we discuss the results of runs 2d-r3 (trad vs NT), 3d-r1 (trad vs NT) and 3d-r3 (NT), analyzing the NT effects and the presence of the unstable jet.

3 Results

3.1 Description of the NIW field

Far from the source, i.e. the storm track, the wave field mainly results from the propagation of a low-mode internal wave (IW). A decomposition of motions at frequency f_0 onto vertical normal modes reveals that about 70 % of the NI energy resides in the first 5 modes corresponding to horizontal scales from 470 km to 68 km (35 % in mode 1).

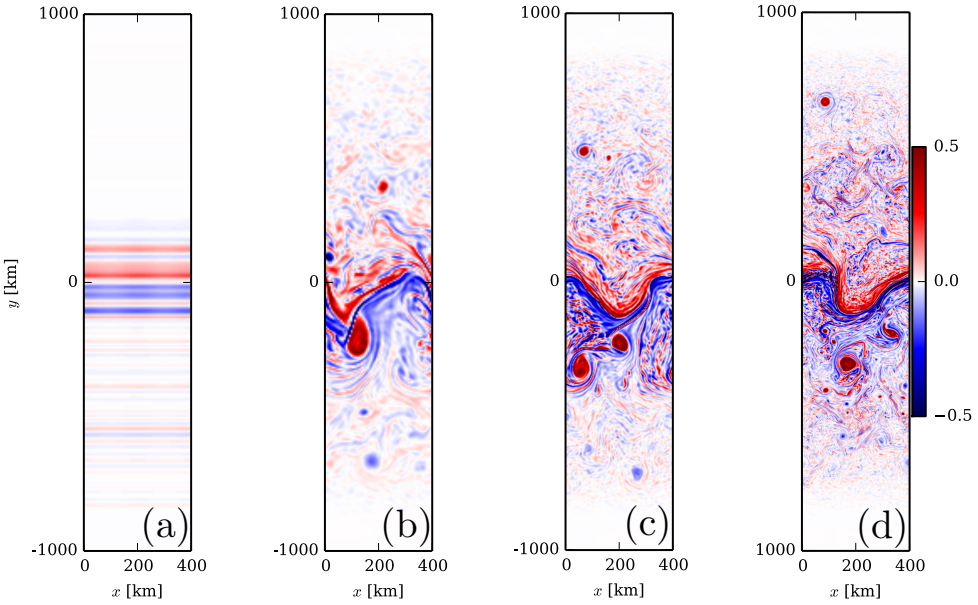

Figure 2: Dimensionless surface vertical vorticity ζ/f_0. Initial state of (a) run 3d-r1, final states of (b) run 3d-r1, (c) run 3d-r2 and (d) run 3d-r3.

Mainly excited at frequency f_0 at the center of the domain, waves propagate away from their source and are damped in the sponge layers at high and low latitudes. Most of the dissipation is effective at the bottom through the linear drag, which arrests the inverse cascade of energy at large scales.

Fig. 3 shows horizontally-averaged kinetic energy spectra at different depths for the NT version of runs 2d-r3 (left) and 3d-r3 (right). The spectra reveal an active IW field predominately at near-inertial frequencies in both 2d and 3d runs. The spectral slope does not match the Garett Munk slope (Garrett and Munk, 1972) in the internal wave band. Here, the slope is steeper (-3 to -4) and this suggests that non-linear wave-wave and wave-vortex interactions are too small to supply the high-frequency spectrum. This result differs from Barkan et al. (2016) where IW were allowed to reflect at lateral wall boundaries, and a shallower frequency spectrum was found. In the 2d case, the wave-wave interactions are mostly linear with spectral peaks at inertial frequency f_0 and its harmonics. In the 3d case, however, the inertial peak is wider and the high frequency band is smoother. In particular the $2f_0$ peak does not exist in our simulations as it does in Danioux et al. (2011), where NIWs and mesoscale flows interact for only a few days after imposition of a wind pulse.

3.2 Meridional propagation of IW

Analysis of the HF motions requires separating the HF motions from the LF ones associated with the mesoscale eddies. For that purpose, we used a moving average over an inertial period $T = 2\pi/f_0$ to obtain the LF field (Danioux et al., 2008). The HF field is then the difference between the total and LF field. The HF meridional velocity is plotted on Fig. 4 (left), as a function of latitude and depth after the statistically steady state has been reached. Associated meridional fluxes at latitudes $y = -400$ km (south) and $y = 400$ km (north) are plotted on the right-hand side of Fig. 4. We compare traditional (Fig. 4a-b) and NT (Fig. 4c-d) versions of runs 2d-r3 and run 3d-r3 (NT) (Fig. 4e-f).

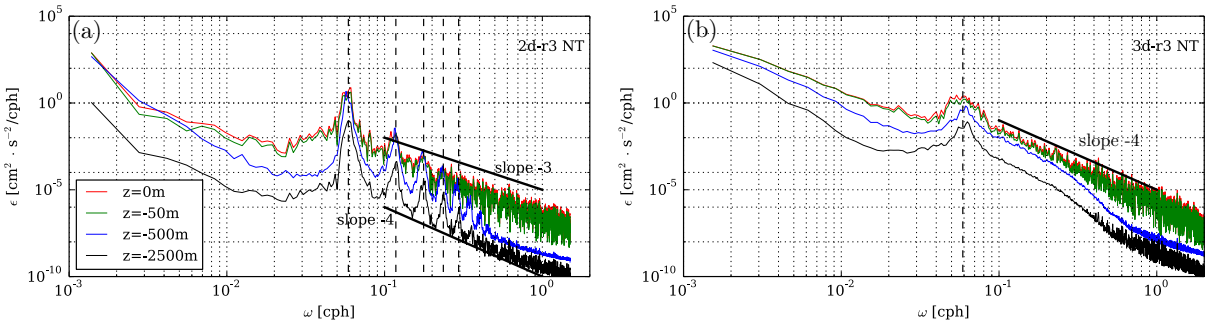

Figure 3: Horizontally-averaged kinetic energy frequency spectra at the surface (red), at $z = -50$ m (green), at $z = -500$ m (blue) and at $z = -2500$ m (black). (a) NT version of runs 2d-r3. (b) run 3d-r3. Dashed back lines represent inertial and harmonic peaks.

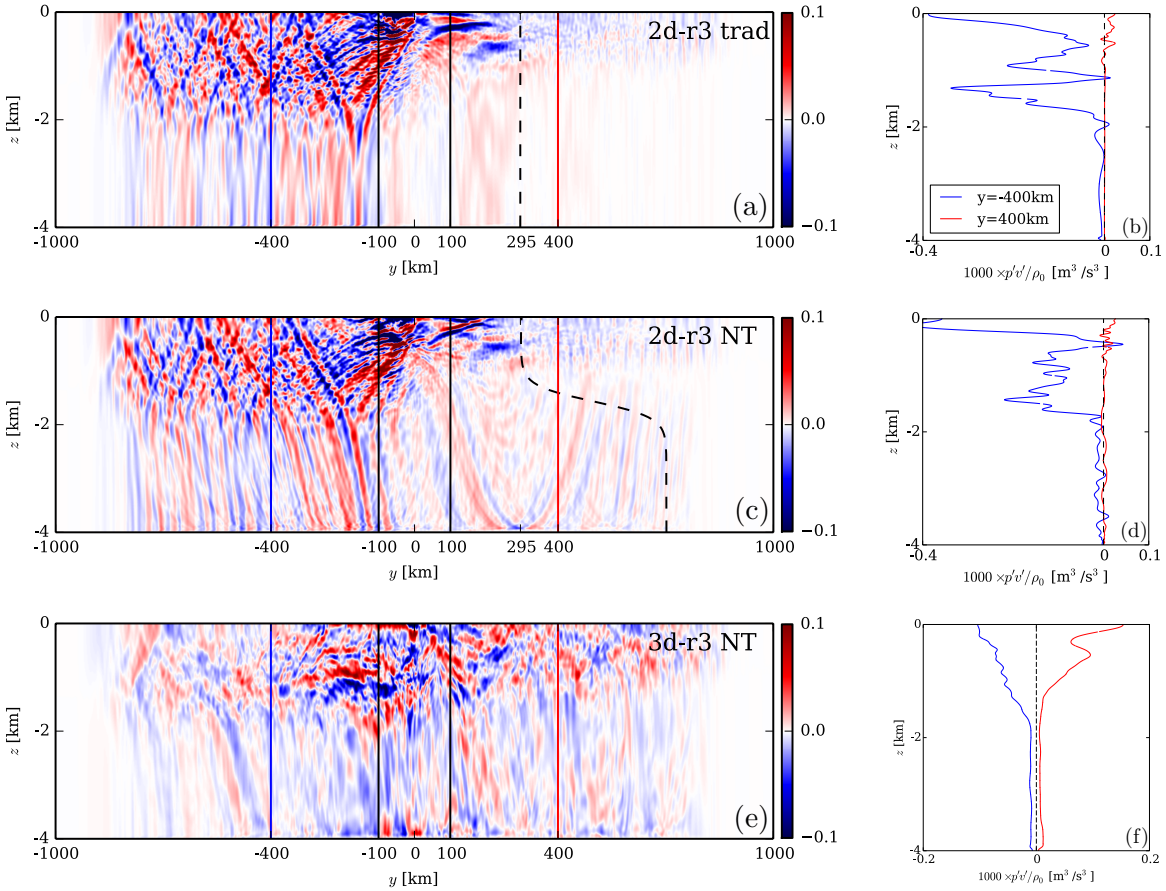

Figure 4: HF part of the meridional velocity as a function of latitude and depth energy at a given time (left panels) and associated time-averaged meridional fluxes (right panels) at fixed latitudes $y = -400$ km (blue) and $y = 400$ km (red). (a)-(b) Traditional version of runs 2d-r3. (c)-(d) NT version of runs 2d-r3. (e)-(f) run 3d-r3. On the left panel, solid black lines represent the meridional extension of the wind forcing. The dashed black lines represent the critical latitude at $y = 295$ km which is depth-dependent while relaxing the TA and allows a poleward propagation of NIWs as a result of critical reflexions.

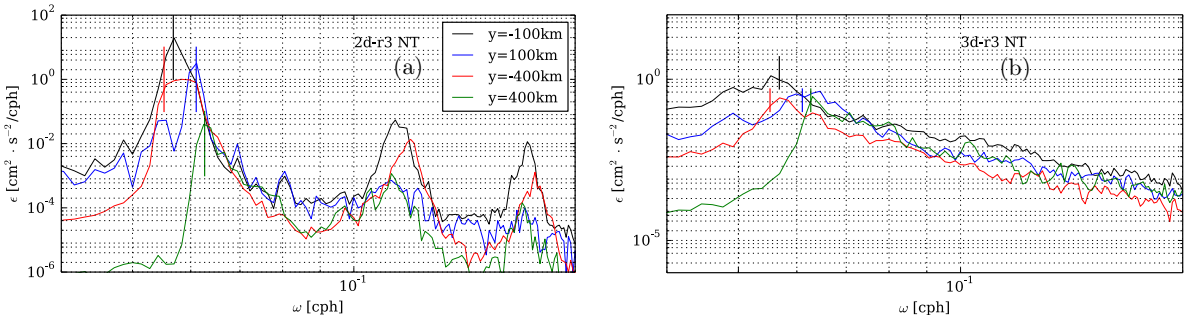

Figure 5: Vertically-averaged kinetic energy frequency spectra at latitudes $y = \pm 100$ km (in the jet) and $y = \pm 400$ km (far from the jet). (a) NT version of runs 2d-r3. (b) run 3d-r3.

As expected within the TA (Fig. 4a), super-inertial frequency waves propagate to the south, until they reach the lateral boundary $y = -L_y/2$ where they are damped. For $y > 0$, we see very slightly super-inertial waves hitting their nearby turning latitudes and a very weak amount of super-inertial waves propagating far from the source. This is confirmed by Fig. 4b, where the HF meridional flux is plotted as a function of depth. Most of the energy propagates equatorward and the flux is concentrated in the upper 2000 m.

Relaxing the TA, we see largely the same picture except that now, sub-inertial waves can and do propagate poleward as noted in Gerkema and Shrira (2005b). As we see on Fig. 4c, waves can be trapped in weakly stratified guides at depth. Critical reflections are visible (for example at $y = 295$ km) as in Winters et al. (2011) where a propagating monochromatic wave was considered. Besides those qualitative differences, most of the HF energy propagates southward as shown in the NT meridional flux plotted on Fig. 4d.

Allowing the jet to develop in 3d and spawn eddies, the solution looks significantly different. NIWs can propagate both poleward and equatorward (Fig. 4e-f). The meridional fluxes at latitudes $y = \pm 400$ km are positive northward and negative southward with a comparable magnitude. When comparing the solutions with and without the TA in runs 3d-r1 (not shown here), we note the same magnitude of meridional fluxes. Therefore significant northward fluxes are not due to NT effects but rather to super-inertial waves excited by the wind forcing, which then propagate northward into our sponge region. Vertically-averaged kinetic energy frequency spectra at latitudes $y = \pm 100, 400$ km are plotted on Fig. 5 for NT version of runs 2d-r3 and run 3d-r3. For the 2d case (left panel of Fig. 5), the inertial peak at $y = 400$ km is almost two decades weaker than the one at latitude $y = -400$ km: a negligible amount of HF energy propagates poleward. However, in 3d, we see an equivalent amount of NI energy at both latitudes $y = \pm 400$ km. NIWs propagating northward are then the results of the combination between energetic mesoscale flows and HF wind forcing which broadens the frequency range of excited waves.

4 Discussion

High-resolution numerical simulations of an idealized mid-latitude ocean have been used to investigate the propagation and the fate of NIWs, excited by a stochastic HF wind forcing. Our simulations incorporate the β-effect, a zonal jet with a meridional vorticity

gradient and a rich field of mesoscale eddies. Furthermore, we have relaxed the TA to analyse the dynamical effects of the horizontal component of the Coriolis force. We show that our NIW field consists mainly of outward radiating low-mode waves of locally super-inertial frequencies.

NT effects After relaxing the TA, ray tracing theory shows that locally sub-inertial waves can propagate further poleward than their critical latitude within weakly stratified wave guides. We show that, within a more realistic context with HF surface wind and mesoscale eddies, the fraction of sub-inertial energy excited is negligible compared to super-inertial energy. Even more exotic wave guides, due to both vertical/meridional gradients of stratification and NT dynamics, are allowed but the fraction of energy within these guides is not significant in our experiments.

Northward meridional fluxes However, in presence of the 3d zonal jet and eddies, a significant amount of energy is able to propagate northward, in contrast to the 2d runs. These meridional fluxes are due to super-inertial waves propagating poleward from their generation site. Further investigation is required to better understand the mechanisms involved in broadening the NI excitation peak by the eddy field that allows this propagation to occur.

References

Anderson, D. L. T. and Gill, A. E. (1979). β-dispersion of inertial waves. *Journal of Geophysical Research*, 84(C4):1836+.

Barkan, R., B, W. K., and C, M. J. (2016). Enhancement of Eddy Kinetic Energy Dissipation by Internal Waves. *Geophys. Res. Let.*

Danioux, E., Klein, P., Hecht, M. W., Komori, N., Roullet, G., and Le Gentil, S. (2011). Emergence of Wind-Driven Near-Inertial Waves in the Deep Ocean Triggered by Small-Scale Eddy Vorticity Structures. *J. Phys. Oceanogr.*, 41(7):1297–1307.

Danioux, E., Klein, P., and Rivière, P. (2008). Propagation of wind energy into the deep ocean through a fully turbulent mesoscale eddy field. *J. Phys. Oceanogr.*, 38(10):2224–2241.

D'Asaro, E. A. (1989). The decay of wind-forced mixed layer inertial oscillations due to the β-effect. *Journal of Geophysical Research*, 94(C2):2045+.

Garrett, C. (2001). What is the near-inertial band and why is it different from the rest of the internal wave spectrum ? *J. Phys. Oceanogr.*, 31(4):962–971.

Garrett, C. J. and Munk, W. G. (1972). Space-Time scales of internal waves. *Geophys. Fluid Dyn.*, 3:225–264.

Gerkema, T. and Shrira, V. I. (2005a). Near-inertial waves in the ocean: beyond the traditional approximation. *Journal of Fluid Mechanics*, 529:195–219.

Gerkema, T. and Shrira, V. I. (2005b). Near-inertial waves on the a non-traditional β-plane. *Journal of Geophysical Research*, 110(C1):1003+.

Klein, P. and Smith, S. L. (2001). Horizontal dispersion of near-inertial oscillations in a turbulent mesoscale eddy field. *Journal of Marine Research*, pages 697–723.

Kunze, E. (1985). Near-inertial wave propagation in geostrophic shear. *J. Phys. Oceanogr.*, 15(5):544–565.

Lee, D.-K. and Niiler, P. P. (1998). The inertial chimney: The near-inertial energy drainage from the ocean surface to the deep layer. *Journal of Geophysical Research*, 103(C4):7579+.

Winters, K. B., Bouruet-Aubertot, P., and Gerkema, T. (2011). Critical reflection and abyssal trapping of near-inertial waves on a β-plane. *Journal of Fluid Mechanics*, 684:111–136.

Winters, K. B. and de la Fuente, A. (2012). Modelling rotating stratified flows at laboratory-scale using spectrally-based DNS. *Ocean Modelling*, 49-50:47–59.

Young, W. R. and BenJelloul, M. (1997). Propagation of near-inertial oscillations through a geostrophic flow. *Journal of Marine Research*, pages 735–766.